

Article Open Access

Multi-omics reveals key cell types and gene families regulating eggshell strength in chicken uteri

Xiao-Ke Zhang¹, Ji-Lan Chen^{1,*}, Yan-Yan Sun¹, Qin Li¹, Peng-Yun Ma¹, Hong-Feng Du¹, Han-Han Yang¹, Xin-Yi Li¹, Xin-Ying Xu¹, Hui Ma¹, Jing-Wei Yuan¹, Yun-Lei Li^{1,*}

¹ State Key Laboratory of Animal Biotech Breeding, Institute of Animal Science, Chinese Academy of Agricultural Sciences, Beijing 100193, China

ABSTRACT

Eggs represent an accessible and nutrient-dense source of high-quality animal protein, and decades of selective breeding have markedly elevated reproductive output in commercial laving hens. However, sustaining elevated productivity while improving eggshell integrity presents a critical challenge, as the molecular mechanisms of eggshell strength remain unclear. In this study, phenotypic assessment of eggshell strength was combined with single-cell transcriptomic profiling of the uterus from highand low-strength groups, transcriptomic analysis of multiple tissues, and quantitative proteomic analysis of uterine fluid. Serum calcium and phosphorus levels did not differ significantly between groups. A single-cell atlas of the Rhode Island Red uterus was successfully generated for the first time, identifying nine distinct cell populations encompassing smooth muscle, epithelial, endothelial, and immune subsets. Integration of transcriptomic and that genes encoding proteomic datasets revealed (COL4A1/2, COL1A1/2, collagens COL5A1, COL6A1/2/3), solute carriers (SLC4A4/7, SLC6A4, SLC9A2/9, and SLC38A2), ATPases (ATP1A1, ATP1B1, ATP2B1/2, ATP2A2/3, and ATP2C1), calcium voltagegated channels (CACNB2, CACNA1C, and CACNA2D1), annexins (ANXA5 and ANXA6), and integrins (ITGB1 and ITGA9) were key molecular determinants associated with variation in eggshell strength. These genes were primarily enriched in signaling cascades involved in focal adhesion, actin cytoskeleton regulation, extracellular matrix (ECM)receptor interactions, and calcium signaling. Notably, collagen family genes were predominantly localized to smooth muscle cells, consistent with the tissue remodeling and uterine inversion that occur during shell calcification, which may enhance spatial proximity between calcium ions

This is an open-access article distributed under the terms of the Creative Commons Attribution Non-Commercial License (http:// creativecommons.org/licenses/by-nc/4.0/), which permits unrestricted non-commercial use, distribution, and reproduction in any medium, provided the original work is properly cited.

Copyright ©2025 Editorial Office of Zoological Research, Kunming Institute of Zoology, Chinese Academy of Sciences

and matrix proteins. These findings establish a multi-omics framework for understanding the uterine regulatory mechanisms underlying eggshell formation and offer a molecular foundation for breeding strategies aimed at prolonging laying cycles while preserving shell quality.

Keywords: Chickens; Eggshell strength; Multi-omics; Single-cell transcriptome; Uterus

INTRODUCTION

Eggs offer a cost-effective, nutrient-dense source of high-quality animal protein. Sustained genetic selection over the past five decades has markedly improved egg production and reproductive efficiency in laying hens. Current breeding programs target prolonged production cycles of up to 100 weeks, with a cumulative output of 500 eggs per hen (Bain et al., 2016). Achieving this benchmark requires not only enhanced productivity but also consistent preservation of egg quality throughout the extended laying period. Egg breakage rates exceeding 5% have been observed during late-stage production in Rhode Island Reds—a Shaver pure line introduced from the University of Guelph in 2018—consistent with prior findings (Liu et al., 2018; Silversides et al., 2007). These challenges underscore the need to improve eggshell quality and integrity while maintaining high productivity.

The eggshell serves as a critical barrier that protects internal contents from microbial contamination, regulates water and gas exchange during embryogenesis, and provides calcium required for embryonic skeletal development. Typically, the shell comprises 10%–11% of the total egg weight (Ar et al., 1979), with a composition of approximately 1.6% water, 95% calcium carbonate in the form of calcite, and 3.3%–3.5% organic substances such as fibrin, collagen, proteoglycans, and glycoproteins (Roland, 1982). Shell formation occurs within the uterus (shell gland), which

Received: 05 August 2025; Accepted: 15 September 2025; Online: 16 September 2025

Foundation items: This work was supported by the China Agriculture Research System of MOF and MARA (CARS-40), Layer Germplasm Resources Conservation of MARA (19221274, 19240847), Agricultural Science and Technology Innovation Program (ASTIP-2021-IAS-16), China Scholarship Council (CSC202303250107, CSC202503250127), and National Germplasm Bank of Domestic Animals (2024)

 ${\tt ^*Corresponding\ authors,\ E-mail: liyunlei@caas.cn;\ chen.jilan@163.com}$

represents the longest stage of the egg formation process, lasting approximately 19 h (Gautron et al., 2021). The biomineralization process is governed by precise temporal and spatial regulation, encompassing three distinct stages: initial nucleation and rapid calcium carbonate deposition (5 h), linear deposition (12 h), and termination of calcification (2 h). The protein composition of the uterine fluid changes dynamically throughout these stages (Gautron et al., 1997), and matrix proteins in the fluid exhibit high calcium-binding affinity, playing a pivotal regulatory role in crystal growth and guiding formation of the palisade layer (Hincke et al., 2000; Soledad Fernandez et al., 2001). This highly organized columnar crystal layer provides the structural rigidity required to resist external mechanical stress and prevent shell fracture. Uterine fluid secretion peaks between 18 h and 19 h post-ovulation (Shapiro et al., 2013). Prior to eggshell formation, the uterus lacks calcium reserves (Nys et al., 1999), relying entirely on a continuous supply from blood plasma during calcification (Gautron et al., 1997).

The eggshell strength trait exhibits moderate to high heritability, indicating substantial genetic influence on shell quality (Chen et al., 2024; Sun et al., 2015). Genome-wide association studies have identified several candidate loci linked to this trait (Chen et al., 2024), including ovocalyxin-32 on chromosome 9, reported through F_2 linkage mapping (Takahashi et al., 2009, 2010). Transcriptomic comparisons between hens with low and normal shell strength identified differential gene expression enriched in focal adhesion, calcium ion transport, and calcium signaling pathways (Zhang et al., 2015). A follow-up study by Zhang et al. (2019) divided 60 Hy-Line Brown hens into high and low shell strength groups and observed no significant differences in serum estradiol (E2) or calcium levels. Proteomic profiling of eggshells from hens at 38 and 108 weeks of age identified 76 differentially expressed proteins involved in adherens junctions, extracellular matrix (ECM)-receptor interactions, focal adhesion, and oxidative phosphorylation (Zhao et al., 2024). Investigations employing physiological assays, genetic markers, histological analyses, and candidate gene studies have contributed to the understanding of shell formation (Brionne et al., 2014; Cheng & Ning, 2023; Sun et al., 2013; Yang et al., 2020; Zhao et al., 2024), yet the genetic architecture controlling eggshell strength remains insufficiently characterized, especially from a multi-omics perspective. This knowledge gap has impeded efforts to optimize extended laying cycles without compromising shell integrity.

The rapid development of single-cell RNA sequencing (scRNA-seq) has transformed the resolution at which transcriptional landscapes in livestock and poultry can be analyzed (Leng et al., 2024; Wang et al., 2024), enabling accurate identification of discrete cell types and improving detection sensitivity (Grün & Van Oudenaarden, 2015). To elucidate the molecular mechanisms underlying variation in eggshell strength, multi-layered analyses were conducted in Shaver pure-line Rhode Island Red hens, integrating phenotypic traits, serum biochemical indices, bulk and single-cell transcriptomics, and uterine fluid proteomics. This study provides a valuable genomic and cellular framework for future functional investigations and contributes foundational resources for the genetic improvement of laying performance in commercial poultry.

MATERIALS AND METHODS

Ethics statement

The present study was approved by the Animal Care and Use Committee of the Institute of Animal Science, Chinese Academy of Agricultural Sciences (IAS-CAAS, No. IAS2023-49) and was performed in accordance with all relevant guidelines and regulations set by Ministry of Agriculture and Rural Affairs of the People's Republic of China.

Animal selection and sample collection

Eggshell strength was evaluated in 806 healthy Shaver pureline Rhode Island Red hens at 33 weeks of age under uniform management conditions, using an egg force reader (FGV-10XY, Orka Food Technology, USA). For each hen, 3–4 eggs were measured consecutively, excluding cracked, soft-shelled, and double-yolked eggs. Based on the resulting distribution (Figure 1A), hens were classified into high and low eggshell strength groups. Six individuals exhibiting an average eggshell strength above 4.5 kg/cm² were assigned to the high-strength group (HTSS), and six individuals with values below 3.3 kg/cm² were assigned to the low-strength group (LTSS). Both groups laid between 60 and 80 eggs, with no significant difference in shell weight observed between them.

From each individual, 2 mL of blood was collected from the wing vein prior to euthanasia. Uterine fluid was harvested at 18–19 h post-ovulation, corresponding to the peak secretion phase, using a 1 mL pipette and transferred into low-adsorption 1.5 mL DNA/RNase-free centrifuge tubes. Protease inhibitors were added immediately following collection. Initial centrifugation was performed at 5 000 r/min and 4°C for 5 min (radius 4 cm) to remove debris. The supernatant was aspirated and transferred to a new centrifuge tube, followed by centrifugation at 12 000 r/min and 4°C for 10 min (radius 4 cm), repeated twice. The final supernatant was aliquoted into new tubes, snap-frozen in liquid nitrogen, and stored for subsequent proteomic sequencing.

Tissue samples (*n*=6 per group) from uterus, red isthmus, magnum, ovary, duodenum, and liver were collected, immediately frozen in liquid nitrogen, and stored at -80°C for subsequent RNA-seq. Uterine samples were partially preserved for single-cell suspension preparation and downstream scRNA-seq. Integrated multi-omics analyses, including phenotype, serum biochemistry, transcriptomics, and proteomics, were performed (Figure 1B).

Determination of serum calcium and phosphorus concentrations

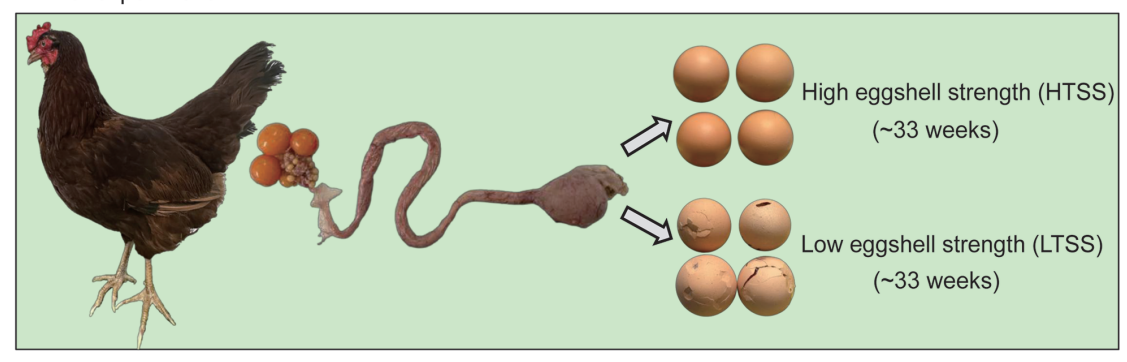
Serum calcium and inorganic phosphorus concentrations were quantified using an automatic biochemical analyzer (CLS880, Jiangsu Zecheng Biotechnology, China). Under alkaline conditions, serum calcium ions were reacted with o-cresol phthalein complexone to form a red-colored complex, with absorbance measured at 600 nm. The increase in absorbance was directly proportional to calcium ion concentration, which was determined by comparison with concurrently processed standards. Under acidic conditions, ammonium molybdate was reacted with inorganic phosphorus in serum to form a non-reducing phosphomolybdic acid compound. Absorbance was measured at 340 nm, and the increase in signal was proportional to inorganic phosphorus concentrations in serum, which was similarly quantified using standard comparisons.

Bulk RNA-seq and data processing

Total RNA was extracted from tissue samples using TRIzol®

1397

A Animal experiment



B Data generation

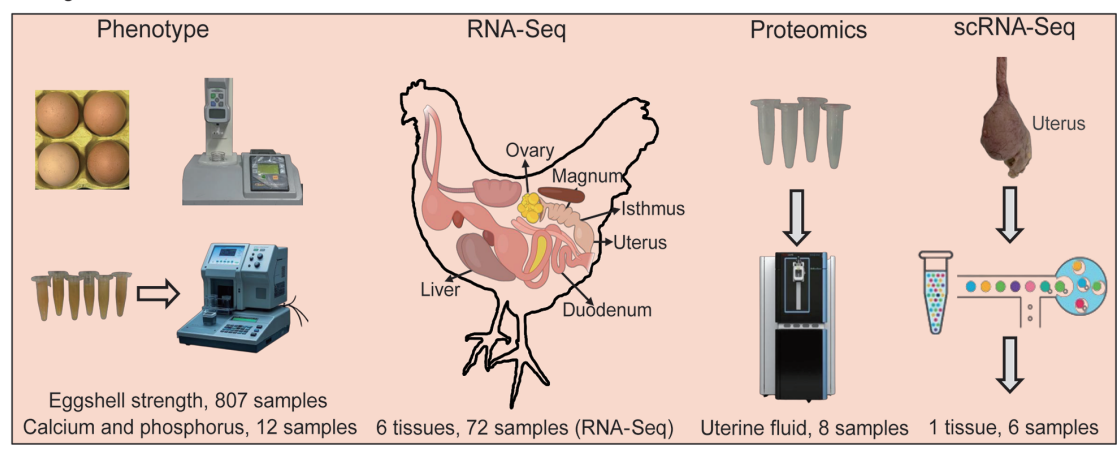


Figure 1 Schematic overview of the study

A: Experimental design. A total of 806 Rhode Island Red chickens were evaluated for eggshell strength at 33 weeks of age. Individuals were divided into high- and low-strength groups based on measured values. B: Sample collection and data generation. Twelve serum samples were collected for biochemical analysis. Six tissue samples were subjected to transcriptomic sequencing and uterus single-cell RNA sequencing. Eight uterine fluid samples were collected for tandem mass spectrometry sequencing.

Reagent following the manufacturer's instructions. RNA quality was determined using a 5300 Bioanalyzer (Agilent, USA), and concentration was measured using a NanoDrop 2000 spectrophotometer (Thermo Scientific, USA). RNA purification, reverse transcription, library construction, and sequencing were performed at Shanghai Majorbio Bio-Pharm Biotechnology (China) following Illumina (USA) protocols. The RNA-seq transcriptome library was prepared using the Illumina® Stranded mRNA Prep, Ligation Kit (Illumina, USA) with 1 µg of total RNA. After quantification using Qubit v.4.0, paired-end libraries were sequenced on the NovaSeq Xplus platform (Illumina, USA).

Raw paired-end reads were trimmed and quality-filtered using Trimmomatic (v.0.39) (Bolger et al., 2014) under default parameters. Clean reads were aligned to the chicken reference genome (GRCg6a, v.112) using HISAT2 (v.2.2.1) (Kim et al., 2019). Two low-quality duodenal samples were excluded, and 70 high-quality samples with more than 20 million clean reads and unique mapping rates above 84% were retained for subsequent analysis (Supplementary Table S1). Gene-level read counts for 30 862 Ensembl-annotated genes (*Gallus gallus* GRCg6a v.112) were extracted using featureCounts (v.2.0.6) (Liao et al., 2014). Differential expression analysis was conducted using the DESeq2 (v.1.42.1) R toolkit. Genes with log₂(fold change) (|log₂FC|)>0.5 and adjusted *P*≤0.05 were considered significantly differentially expressed genes (DEGs). Functional

enrichment analysis was performed using Database for Annotation, Visualization, and Integrated Discovery (DAVID v.2024q4, https://davidbioinformatics.nih.gov/summary.jsp).

RNA isolation and quantitative reverse transcription polymerase chain reaction (RT-qPCR)

Total RNA was extracted using an RNAfast200 Kit (Fastagen, China), and RNA concentration was quantified using a NanoDrop 2000 spectrophotometer (Thermo Fisher Scientific, USA). In total, 1 000 ng of RNA was reverse-transcribed into complementary DNA (cDNA) using the PrimeScript RT Reagent Kit (TaKaRa, Japan). qRT-PCR was conducted using TB Green® Premix Ex Taq $^{\text{TM}}$ II (Tli RNaseH Plus, TaKaRa, Japan) on the CFX96 Touch Real-Time PCR System (Bio-Rad, USA), with three technical replicates for each reaction. Relative mRNA expression levels were calculated using the $2^{-\Delta\Delta Ct}$ method, with β-actin as the internal reference gene. Primer sequences are provided in Supplementary Table S2.

Single-cell tissue dissociation and cell purification

Uterus tissue was washed in sterile 1× Dulbecco's phosphate-buffered saline (DPBS) and minced on ice in a sterile culture dish. Enzymatic dissociation was performed using a solution containing 0.25% trypsin and 10 μ g/mL DNase I dissolved in PBS with 5% fetal bovine serum (FBS; Cat. no. SV30087.02, Thermo Fisher, USA). Tissue digestion was carried out at 37°C with gentle shaking at 50 r/min for 40 min. To increase yield and viability, dissociated cells were harvested at 20 min

intervals. Cell suspensions were filtered through a 40 µm nylon cell strainer, and red blood cells were removed using 1× red blood cell lysis solution. The dissociated cells were washed with 1× DPBS containing 0.4% FBS. Cell viability was assessed using 0.4% acridine orange/propidium iodide (AO/PI) staining on a Countstar Rigel S2 system (Countstar, China). Processed samples were then submitted to Majorbio Bio-Pharm Technology (China) for downstream analysis.

Single-cell 10× library construction and sequencing

Beads containing unique molecular identifiers (UMIs) and cellspecific barcodes were loaded to near-saturation levels to ensure one bead per cell within individual gel beads-inemulsion (GEM) droplet. Following cell lysis, polyadenylated RNA transcripts hybridized to the oligo-dT primers on the beads. Beads were then pooled into a single tube for reverse transcription. During cDNA synthesis, each transcript was labeled at the 3' end (5' end of an mRNA transcript) with a UMI and a cell barcode, preserving the molecular and cellular origin. The resulting cDNA underwent second-strand synthesis, adaptor ligation, and amplification to generate sequencing libraries enriched for the 3' ends of transcripts. Library construction was performed according to the standard Chromium Single Cell 3' (v.3.1) protocols, which captures whole-transcriptome profiles while linking each read to its corresponding cell and transcript. Final libraries were quantified using a High Sensitivity DNA Chip (Agilent, USA) on a Bioanalyzer 2100 and the Qubit High Sensitivity DNA Assay (Thermo Fisher Scientific, USA). The libraries were sequenced on the NovaSeq Xplus platform (Illumina, USA) using 2×150 chemistry. Sequencing was performed by Majorbio (China).

ScRNA-seq data processing and analysis

Raw sequencing reads were processed using Cell Ranger (v.8.0.1) with default and recommended parameters. FASTQ files generated from Illumina output were aligned to the GRCg6a (v.112) chicken reference genome using the STAR algorithm (Dobin et al., 2013). Gene-barcode matrices were generated for each individual sample by counting UMIs and filtering non-cell associated barcodes. The resulting matrices, containing gene expression profiles for barcoded cells, were imported into Seurat (v.5.1.0) for quality control and downstream analysis. Cells were retained if they met the following criteria: <5 000 detected genes, <20 000 detected transcripts, <25% of reads mapped to mitochondrial genes, and <40% of reads mapped to ribosomal genes. Putative doublets were removed using DoubletFinder (v.2.0.4) with a doublet detection rate of 7.6% (McGinnis et al., 2019). Normalization was performed using the NormalizeData function, followed by identification of highly variable genes (i.e., variable features) with FindVariableFeatures. Data scaling was conducted using the ScaleData function. To eliminate batch effects, single-cell datasets were integrated using the Harmony algorithm via the IntegrateLayers function. Dimensionality reduction was carried out using principal component analysis (PCA), retaining the top 30 principal components. Uniform Manifold Approximation and Projection (UMAP) was applied for two-dimensional visualization of cell clusters. Clusters were identified based on transcriptional similarity and visualized using UMAP, which offers rapid computation, robust reproducibility, and high fidelity in representing cellular structure (Becht et al., 2019). Marker genes distinguishing each cluster were identified using

FindAllMarkers. Cell type annotation was performed using SingleR (v2.4.1), supplemented by manual curation based on reference databases CellMarker and PanglaoDB.

Differential expression and functional enrichment analysis

DEGs between sample groups or cell clusters were identified using the FindMarkers function in the Seurat package, utilizing the likelihood ratio test. Specifically, genes with $|\log_2FC|>1$ and adjusted $P \le 0.05$ were regarded as significant DEGs. Compared to bulk RNA-seq, single-cell transcriptomics generates substantially larger data volume and cellular heterogeneity; thus, more stringent quality control criteria were implemented in this study to ensure robust and biologically meaningful differential expression results.

Gene Ontology (GO) and Kyoto Encyclopedia of Genes and Genomes (KEGG) pathway enrichment analyses were conducted to assess functional categories and signaling pathways significantly associated with the DEGs. Enrichment analyses were performed using DAVID (v.2024q4, https://davidbioinformatics.nih.gov/summary.jsp).

Pseudotime series analysis

Pseudotime analysis was performed using the Monocle2 R package (v.2.34.0). CellDataSet objects were initially created using the newCellDataSet function, with normalization subsequently performed using estimateSizeFactors and estimateDispersions. Low-quality genes (expression<0.1) were filtered using detectGenes. Feature genes for trajectory inference were selected via the setOrderingFilter function. Dimensionality reduction was performed using reduceDimension, followed by cell ordering with orderCells to reconstruct the developmental trajectory across pseudotime.

Cell-cell communication analysis

Cell-cell communication analysis was conducted using CellChat (v.1.6.1). Normalization of expression data was performed using the GetAssayData function, followed by construction of a CellChat object with createCellChat. The curated CellChatDB database was used for in-depth analysis of cell-cell communication. Communication probability and signaling network strength were inferred using the computeCommunProb function to reconstruct the intercellular communication landscape.

Proteomic sequencing and data processing

Samples were lysed in a buffer containing 8 mol/L urea and 1% sodium dodecyl sulfate (SDS) supplemented with appropriate protease inhibitors to prevent protease activity. Protein concentration in the supernatant was determined using the bicinchoninic acid (BCA) method with a BCA Protein Assay Kit (Thermo Scientific, USA), following the manufacturer's protocols. After quantification, proteins were separated by sodium dodecyl-sulfate polyacrylamide gel electrophoresis (SDS-PAGE) and digested with trypsin at a 1:50 trypsin-to-protein mass ratio. The resulting peptides were dried under vacuum and quantified using a NanoDrop One spectrophotometer (Thermo Scientific, USA). Based on peptide concentrations, samples were analyzed using a Vanguish Neo UHPLC system coupled to an Orbitrap Astral mass spectrometer (Thermo Scientific, USA) at Majorbio Bio-Pharm Technology (China).

Raw DIA data were processed using Spectronaut (v.19) (Martinez-Val et al., 2021). Search parameters were set as follows: peptide length 7–52 amino acids; trypsin/P enzyme

cutting site; maximum number of missed cleavage sites 2; carbamidomethylation of cysteines set as a fixed modification; oxidation of methionines and protein N-terminal acetylation set as variable modifications; protein false discovery rate (FDR)≤ 0.01; peptide FDR≤0.01; peptide confidence≥99%; and extracted ion chromatogram (XIC) width ≤75 ppm. Protein quantification was performed using the MaxLFQ method (Cox et al., 2014).

Differentially expressed proteins were defined by: $\log_2 FC > 2$ (up-regulated) or $\log_2 FC < 0.5$ (down-regulated) with adjusted P < 0.05. Functional annotation and enrichment analyses for GO terms and KEGG pathways were conducted for all identified proteins. Protein-protein interaction (PPI) analysis was performed using the UniProt database (Release 2025_01, https://www.uniprot.org/).

Western blotting

Uterine fluid samples were analyzed for COL6A2 and ACTN4 protein expression. Protein concentrations were determined using a BCA Protein Assay Kit (Cwbio, China), and equal amounts of protein were resolved by SDS-PAGE and transferred to polyvinylidene difluoride membranes (Merck Millipore, Germany). Membranes were blocked with 5% nonfat milk in PBS containing Tween-20 for 2 h, then incubated at 4°C overnight with primary antibodies (1:1 000): rabbit anti-COL6A2 (Abcam, UK), rabbit anti-ACTN4 (ABclonal, China), and rabbit anti-GAPDH (ABclonal, China). After washing, membranes were incubated with secondary antibodies

(1:10 000) for 2 h at room temperature. Gray scale values of the bands were calculated using ImageJ (https://imagej.net/ij/) and normalized to GAPDH.

RESULTS

Phenotypic traits and serum biochemical parameters

Among 2 376 eggs assessed from 806 Rhode Island Red hens, mean eggshell strength was 3.88 kg/cm² (Figure 2A). Based on this distribution, six individuals from the high- and low-strength groups were selected, respectively. A significant difference in eggshell strength was observed between these groups (*P*<0.01; Figure 2B), while no significant difference was found in egg weight (Figure 2C). Upon dissection, all 12 hens had eggs present in the uterus at the rapid mineralization stage, and group-specific differences in shell strength were already evident at this point (Supplementary Figure S1). No significant differences were detected in serum calcium, phosphorus, or calcium-to-phosphorus ratio (Figure 2D–F), although mean calcium concentration was elevated in the HTSS group compared to the LTSS group.

Transcriptomic, proteomic, and biochemical data overview

A total of 70 bulk RNA-seq libraries were generated from six major tissues (Supplementary Table S3), yielding approximately 1.5 billion clean reads. The mean unique mapping rate across samples was 89.95% (range:

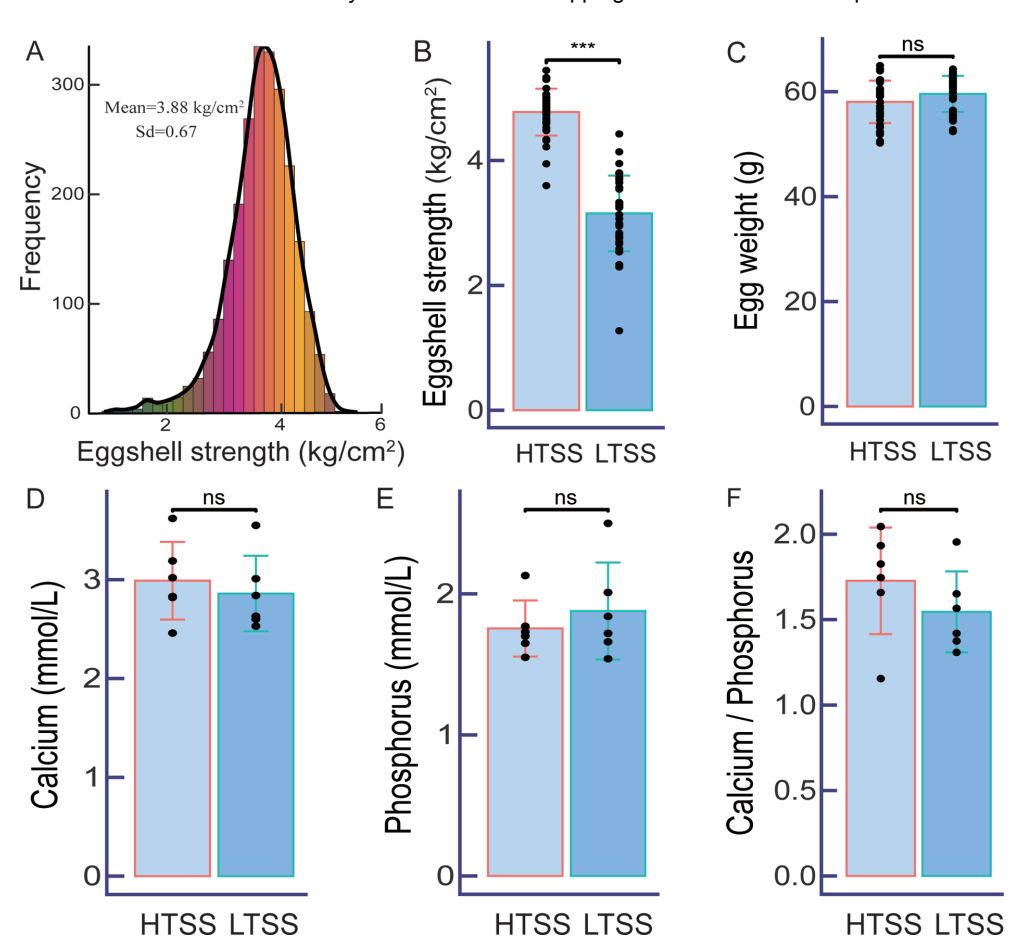


Figure 2 Phenotypic and serum biochemical parameters

A: Distribution histogram of 2 376 eggshell strength measurements across 806 Rhode Island Red chickens. B, C: Distributions of eggshell strength and egg weight in high- (HTSS) and low-strength (LTSS) groups. D–F: Distributions of serum calcium, phosphorus, and calcium-to-phosphorus ratio in HTSS and LTSS groups. ns: Not significant; ***: P<0.001.

77.29%-92.92%) and the mean overall mapping rate was 95.21% (range: 81.58%-97.97%) (Supplementary Table S1). ScRNA-seg of uterine tissue from six HTSS and six LTSS individuals produced six additional datasets (Supplementary Table S3). After rigorous quality control, approximately 2.0 billion clean reads were retained, with an average confident mapping rate of 93.60% (range: 92.60%-95.70%) (Supplementary Table S4). Additionally, eight proteomic datasets were generated from uterine fluid samples collected from HTSS and LTSS hens, using tandem mass spectrometry (Supplementary Table S3). After raw data processing, an average of 3 917 proteins (range: 3 874-3 977) were identified per sample (Supplementary Figure S2). To evaluate biochemical differences associated with eggshell formation, serum calcium and phosphorus levels were measured in 12 samples (six per group) (Supplementary Table S5).

Single-cell clustering and cell type identification

A high-resolution single-cell atlas of the Rhode Island Red chicken uterus was constructed (Figure 3A). Correlation heatmaps for the single-cell datasets are shown in Supplementary Figure S3. Quality control was performed based on key metrics, including the number of detected features (nFeature), total RNA molecule counts (nCount), and the percentages of mitochondrial and ribosomal gene expression (Supplementary Figure S4). Subsequently. putative doublets were identified and (Supplementary Figure S5). Following batch-effect correction, the UMAP plot of the integrated dataset is shown in Supplementary Figure S6. After filtering, 31 596 high-quality single cells expressing 20 507 genes were retained for downstream analyses (Supplementary Table Unsupervised clustering revealed 22 transcriptionally distinct cell clusters (Figure 3A). Manual annotation of these clusters was performed using reference-based classification with the SingleR toolkit and CellMarker database. These cell clusters were subsequently annotated into nine major cell types, including natural killer T cells (13.67%), epithelial cells (37.17%), monocytes (8.75%), smooth muscle cells (17.72%), B cells (7.81%), microglial cells (5.70%), endothelial cells (5.52%), T cells (2.81%), and dendritic cells (0.85%) (Figure 3B). The HTSS and LTSS groups contained 14 599 and 16 955 cells, respectively (Figure 3C). Notable differences in cell type proportions were observed between the HTSS and LTSS groups: epithelial cells were less abundant in the HTSS group, while smooth muscle and endothelial cells were proportionally enriched. Group-specific UMAP visualizations are shown in Figure 3D, and dataset-specific projections for each sample are shown in Supplementary Figure S7. Expression levels and detection frequencies of marker genes across identified cell types are presented in a dot plot matrix (Figure 3E).

Functional enrichment analysis of DEGs in single-cell datasets

A total of 4 123 DEGs were identified across single-cell populations and subjected to GO and KEGG functional enrichment analyses (Supplementary Table S7). Key signaling and structural pathways were visualized (Figure 4A), with cell type—specific DEG profiles detailed in Supplementary Table S8. Multiple gene families were prominently enriched in biologically relevant categories. Collagen family genes (COL1A1, COL1A2, COL4A2, COL4A1, COL6A2, COL6A3, and COL5A1) were strongly associated with the focal

adhesion pathway and encode structural proteins critical for collagen formation. Similarly, ATPase family genes (ATP1A1, ATP1B1, ATP2C1, ATP2B2, ATP2A3, ATP2B1, and ATP2A2) were significantly enriched in calcium ion transmembrane transport and ATP-binding molecular function terms, consistent with their roles in establishing electrochemical gradients and regulating calcium homeostasis. Solute carrier family genes (SLC9A9, SLC6A6, SLC4A7, SLC9A2, and SLC4A4) were enriched in the "plasma membrane" cellular component category and contribute to inorganic cation/anion and amino acid/oligopeptide transport and Rho GTPase signaling cascades. Furthermore, calcium voltage-gated channel family genes (CACNB2, CACNA1C, and CACNA2D1) were enriched in the "L-type voltage-gated calcium channel complex" cellular component category and regulate calcium current density and channel kinetics.

Volcano plots were generated to highlight DEGs at the cell type level (Figure 4B), and expression patterns of selected DEGs across different cell types were visualized (Figure 4C). Collagen family genes showed predominant expression in smooth muscle cells, with COL4A2 and COL4A1 also highly expressed in endothelial cells. CACNA2D1 exhibited strong expression in endothelial populations. While ATPase and solute carrier family genes were broadly expressed across multiple lineages, ATP1A1 and ATP2B2 showed elevated expression in smooth muscle and epithelial cells.

Group-wise comparisons revealed higher expression of collagen and calcium channel genes in the HTSS group relative to the LTSS group, as shown in the heatmap (Figure 4D). To further explore molecular pathways associated with eggshell strength variation, KEGG enrichment was performed at the proteomic level (Figure 4E). Collagen family genes were mainly enriched in focal adhesion and ECMreceptor interaction pathways. ATPase family genes were primarily enriched in adrenergic signaling in cardiomyocytes, cardiac muscle contraction, and calcium signaling pathways. Calcium voltage-gated channel family genes were enriched in gonadotropin-releasing hormone (GnRH) signaling pathway. The PPI network constructed from the DEGs highlighted dense clustering of nodes in the lower right quadrant, with collagen genes exhibiting strong connectivity with integrin alpha and beta subunit genes (Figure 4F).

Pseudotime and cell-cell communication analysis

The distribution of cell types along the pseudotime trajectory revealed dynamic shifts in cell state progression (Figure 5A). Smooth muscle and endothelial cells exhibited peak densities between pseudotime values of 10 and 20, suggesting elevated representation of these populations during this developmental interval. Smooth muscle cells were further subclustered, and PCA distinguished discrete transcriptional states (Figure 5B). BMP2-related tissue stem cells were predominantly enriched in State 1, while differentiated smooth muscle cells were concentrated in State 2. In contrast, State 3 showed a heterogeneous mix of cell types with no dominant lineage signature. Examination of collagen gene expression dynamics was conducted across pseudotime cell-type-specific transcriptional programs: COL1A1 and COL1A2 were highly expressed in differentiated smooth muscle cells (vit_D), whereas COL4A1 and COL4A2 were highly expressed in BMP2-associated tissue stem cells (Figure 5C).

Cell-cell interactions were inferred by quantifying interaction counts and signal strength across all cell types (Figure 5D, E).

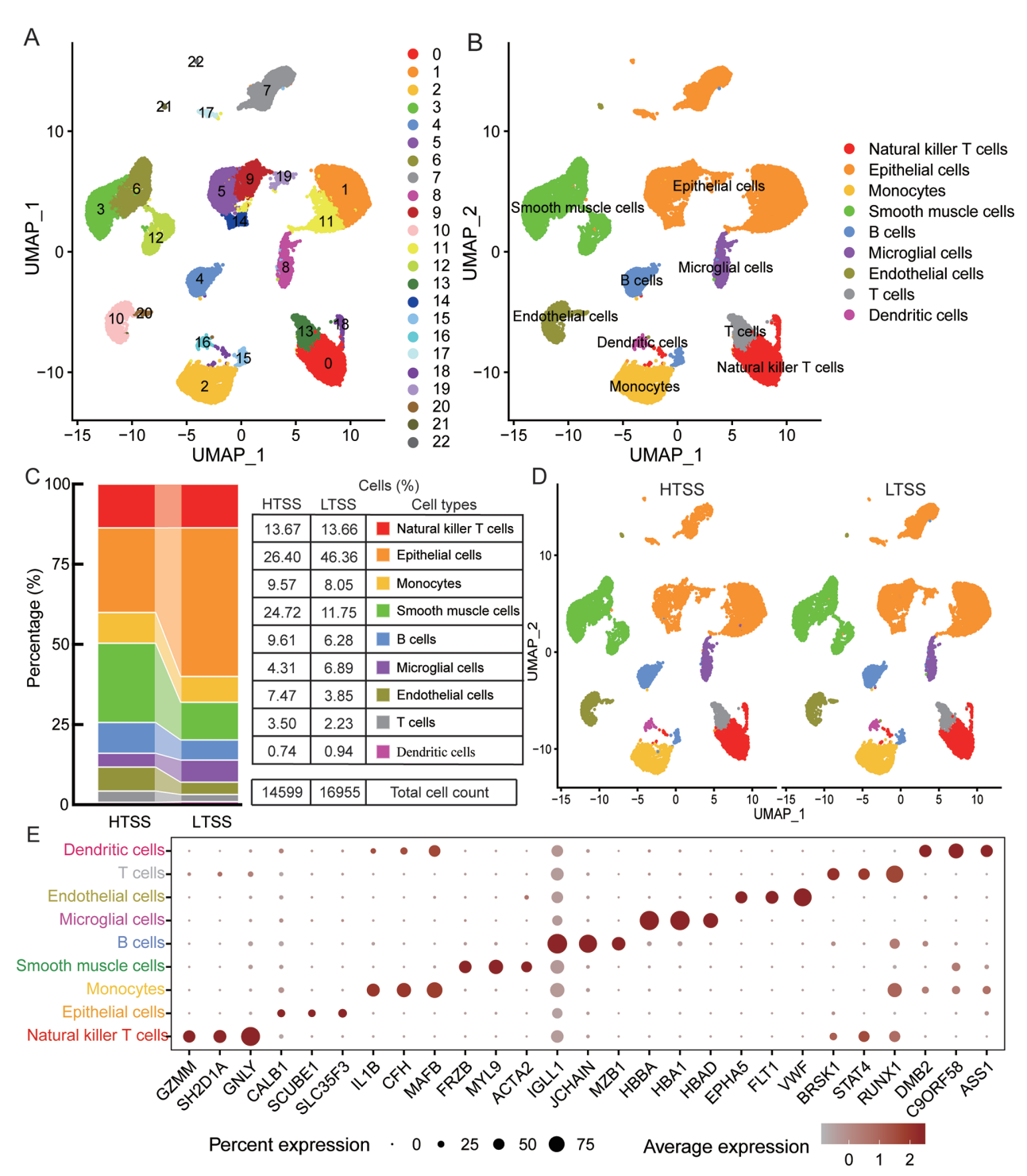


Figure 3 Single-cell transcriptome landscape of the Rhode Island Red chicken uterus

A: UMAP projections identifying 22 specific clusters representing the uterus cell types. B: UMAP projections showing nine major uterine cell types. C: Percentage of cell types in high- (HTSS) and low-strength (LTSS) groups. D: UMAP projections for HTSS and LTSS groups. E: Feature gene expression levels and proportions across cell types.

Smooth muscle cells demonstrated extensive interaction networks, particularly with immune populations including natural killer T cells, T cells, B cells, and monocytes, as well as endothelial cells. Signal transmission patterns were further partitioned into outgoing and incoming communication profiles (Figure 5F). Smooth muscle cells were characterized by prominent outgoing signaling through collagen ligands, while epithelial cells exhibited diverse outgoing signals involving molecules such as amyloid precursor protein (APP) and

fibronectin 1 (FN1). Immune cells (natural killer T cells, T cells, B cells, and monocytes) displayed strong incoming signaling activity across multiple signaling molecules, indicating that these immune cells are relatively active in receiving external signals. Notably, collagen signaling exerted pronounced influence on endothelial cells (Supplementary Figure S8).

Transcriptomic profiling of uterus, isthmus, and duodenum tissues

Differential gene expression analysis was performed across

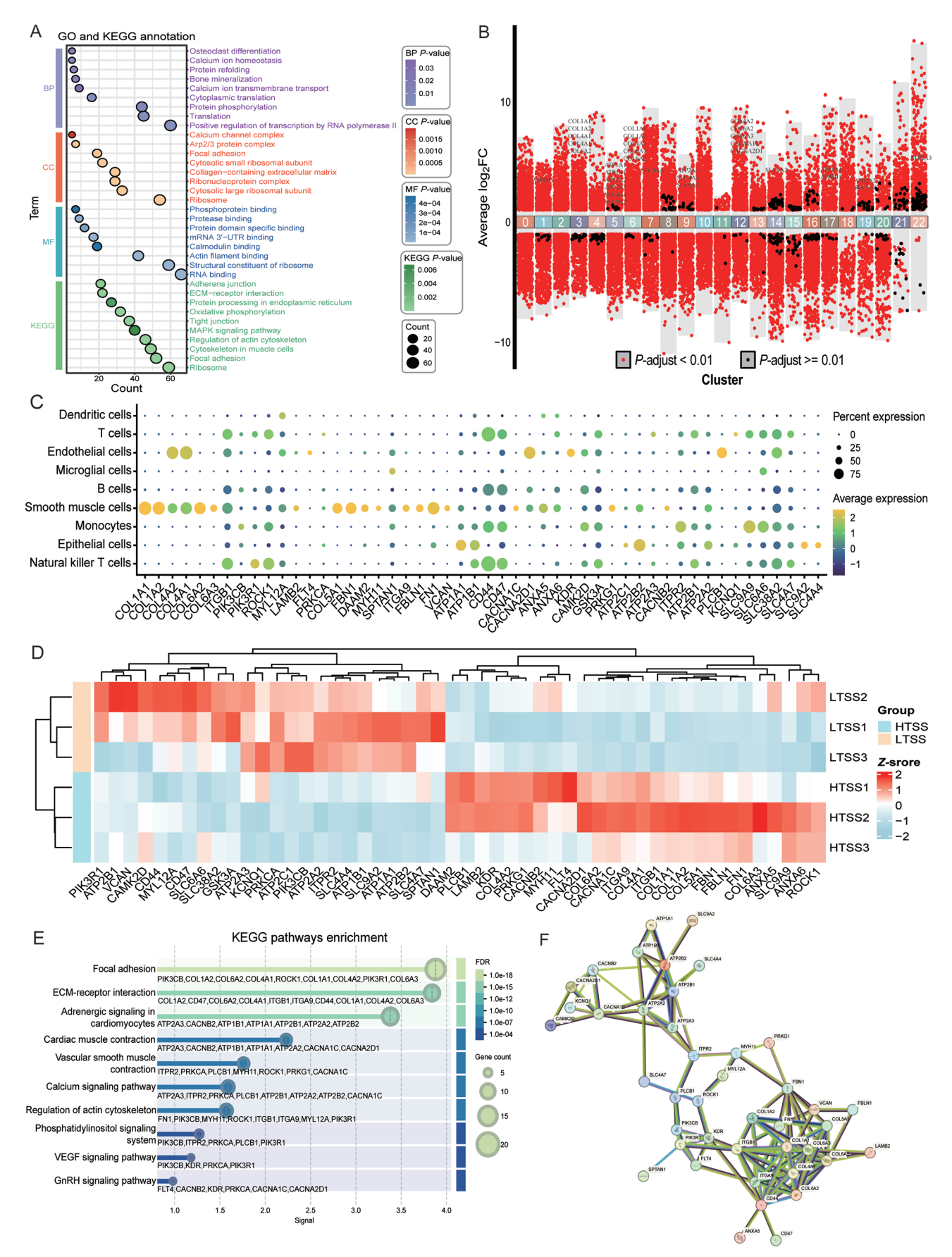


Figure 4 Differentially expressed genes (DEGs) of single-cell datasets in the Rhode Island Red chicken uterus

A: GO and KEGG functional enrichment analyses of DEGs. B: Up-regulated and down-regulated genes across all clusters. x-axis represents clusters 0 to 22, y-axis indicates average log_2FC . C: Expression levels of DEGs in different cell types. D: Expression levels of DEGs in high- and low-strength groups. E: KEGG pathway enrichment analysis of DEGs at the protein level. F: Protein-protein interaction network of DEGs.

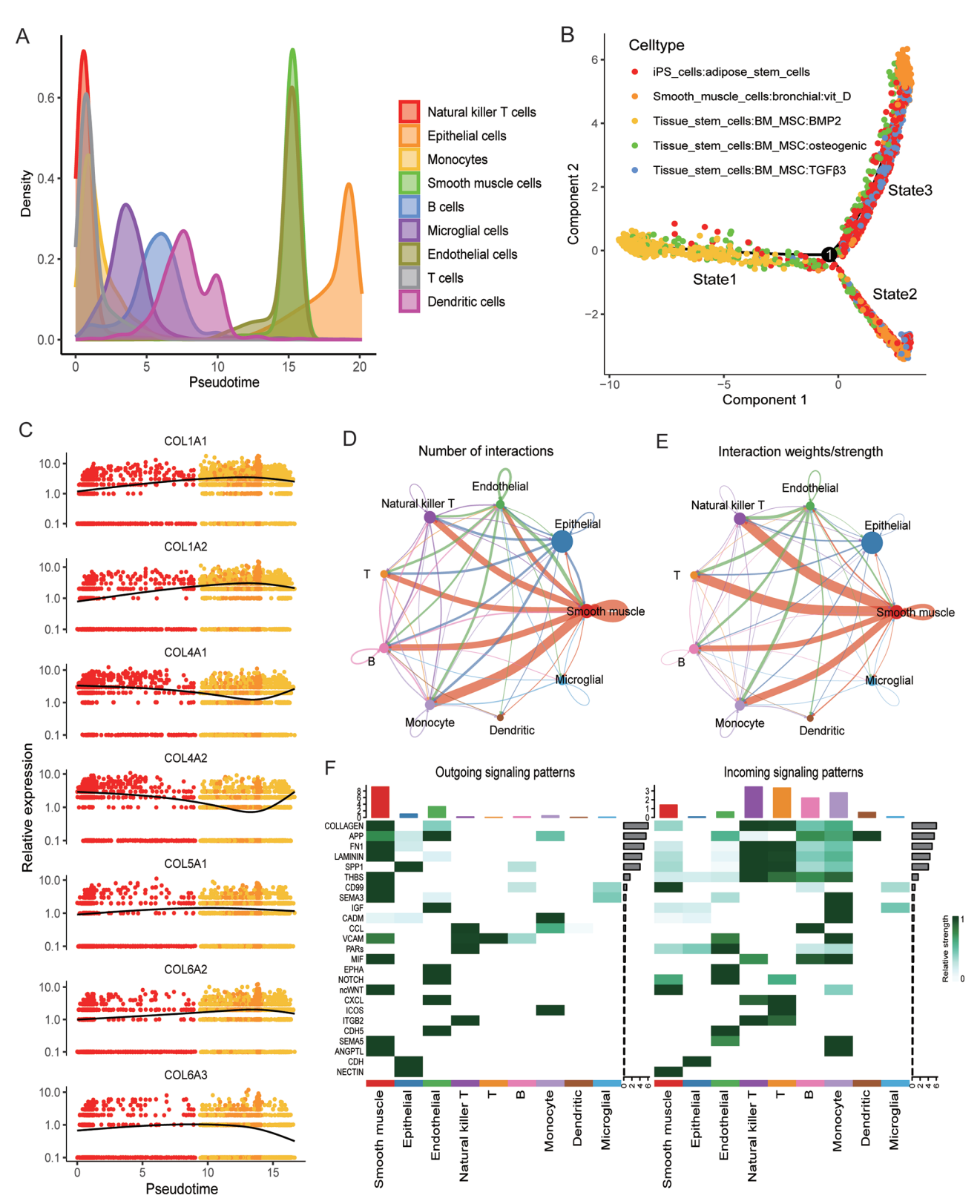


Figure 5 Pseudotime trajectory and cell-cell communication analysis

A: Cell density distribution along pseudotime for all cell types. B: Principal component plot of smooth muscle cells. Each dot represents a single cell, color-coded by timepoints. C: Collagen family gene expression changes over pseudotime. D: Number of cell-cell interactions per cell type. E: Weights/strengths of cell-cell interactions for all cell types. Each color represents a different cell type, arrows represent order, and line thickness represents number/weight. F: Heatmap of outgoing and incoming signaling contributions by cell type; rows represent pathways, columns represent cell types, and color intensity indicates communication probability.

six tissues from the HTSS and LTSS groups. Minimal transcriptomic divergence was observed in the magnum and ovary, with only a few DEGs identified, while no significant

differences were detected in the liver tissues (Supplementary Figure S9). In contrast, substantial transcriptional changes were observed in the uterus, red isthmus, and duodenum

tissues-three tissues involved in eggshell calcification (Figure 6A-C). GO and KEGG enrichment analyses were subsequently performed for the DEGs in these three tissues (Supplementary Table S9), with representative enriched pathways visualized in Figure 6D-F. Enrichment of terms such as "cell adhesion" and "protein binding" across all three tissues indicated a shared functional signature linked to eggshell formation. In the uterus, DEGs, including PDGFRB, ROCK1, ITGA4, ITGB3, COL1A2, COL6A1, COL6A3, and MYL9, were significantly enriched in the focal adhesion pathway, consistent with the patterns observed in the singlecell transcriptomic dataset (Supplementary Table S9). In the duodenum, annexin family genes (ANXA1, ANXA2, ANXA13, ANXA5, and ANXA7) were enriched in the calcium-dependent phospholipid binding pathway, while PANX1, ANXA2, ANXA5, and CACNA2D3 were enriched in the calcium channel activity pathway (Supplementary Table S9). In the uterus, DEGs were significantly enriched in the focal adhesion pathway, muscle cell cytoskeleton, and adherens junctions, consistent with the single-cell DEG results. Quantitative analysis of mRNA levels revealed significantly higher expression of ROCK1, COL6A1, COL6A3, COL4A2, and COL1A1 in the HTSS group compared to the LTSS group, but no significant difference for COL6A2 (Figure 6G).

Proteomic profiling of uterine fluid

By calculating the correlation coefficients between the protein expression levels of samples within groups and those between groups, differences in the proteomes between groups were identified, while the proteomes within groups were relatively stable (Figure 7A). A total of 264 proteins exhibited differential expression, including 168 up-regulated and 96 down-regulated proteins (Figure 7B). KEGG pathway enrichment analysis revealed that these proteins primarily associated with metabolic pathways, endocytosis, MAPK signaling, regulation of actin cytoskeleton, and focal adhesion (Figure 7C), similar to the enriched pathways obtained from transcriptomic analysis (Figure 6D). Within the focal adhesion pathway, the COL6A2 protein showed elevated expression in the HTSS group (Figure 7D). The COL6A1 and OVA proteins also differed between the groups (Supplementary Table S10). Western blotting confirmed significantly higher expression of ACTN4 and COL6A2 proteins in the HTSS group compared to the LTSS group (P<0.05; Figure 7E, F).

DISCUSSION

Rhode Island Reds represent a globally recognized dualpurpose breed valued for both egg-laying performance and favorable meat quality. Their widespread use reflects robust adaptability and productivity under diverse environmental conditions (Zhang et al., 2024). Eggshell strength is a key reproductive trait in poultry production, critically affecting hatchability, transport resilience, and economic output. This trait is governed by a complex interplay of genetic and environmental factors and remains a principal target of artificial selection in layer breeding programs. Previous studies have implicated multiple gene families in modulating eggshell mechanical properties, including collagens (Sun et al., 2023; Zhang et al., 2015), solute carriers (Bahadoran et al., 2018; Li et al., 2025), ATPases (Cui et al., 2025; Gloux et al., 2019; Jonchère et al., 2012; Zhang et al., 2022), calcium voltagegated channels (Li et al., 2021), annexins, and integrin subunits. In the present study, integrated multi-omics analyses

elucidated key molecular determinants of eggshell strength in Rhode Island Reds. Complementary single-cell transcriptomic profiling further enabled high-resolution mapping of uterine states and lineage-specific gene expression signatures. Results indicated that candidate genes associated with eggshell strength were primarily associated with focal adhesion, actin cytoskeleton regulation, ECM-receptor interaction, and calcium signaling.

Transcriptomic profiling of reproductive system tissues, including the liver, ovary, magnum, red isthmus, and uterus, was conducted to elucidate molecular mechanisms underlying variation in eggshell strength in laying hens. Minimal differential gene expression was observed in the magnum and ovary, with no detectable changes in liver tissues. In contrast, pronounced transcriptional differences were identified in the uterus and red isthmus, which both play crucial roles in eggshell mineralization. DEGs were predominantly enriched in pathways linked to focal adhesion, actin cytoskeleton regulation, apoptosis, ECM-receptor interaction, and protein binding. Among these, ROCK1 and multiple collagen family genes were significantly enriched in the focal adhesion and ECM-receptor interaction pathways, aligning with earlier findings (Zhang et al., 2015). gRT-PCR analysis confirmed that expression levels of ROCK1 and key collagen genes were elevated in individuals with high eggshell strength compared to those with low eggshell strength.

To resolve the cellular origin of these molecular signals, single-cell transcriptomic sequencing was performed on uterine tissue samples collected 18-19 hours postovulation-coinciding with peak uterine fluid secretion and rapid eggshell mineralization. This analysis produced the first single-cell transcriptomic atlas of the Rhode Island Red chicken uterus, identifying nine distinct cell types grouped into four major categories: smooth muscle, epithelial, endothelial, and immune cells. These categories mirrored those previously reported in the human endometrium (Marečková et al., 2024; Wang et al., 2020). Integration of single-cell, bulk transcriptomic, and proteomic datasets revealed candidate genes associated with eggshell strength, with collagen gene expression localized predominantly to smooth muscle cells. This pattern may reflect a mechanistic role in uterine wall inversion during eggshell calcification, facilitating optimal integration of calcium ions with matrix proteins. Cell-cell communication analyses indicated that smooth muscle cells maintained extensive signaling interactions with immune, epithelial, and endothelial cells, and functioned as important effectors of collagen signaling pathways. Subpopulations of smooth muscle cells enriched for BMP2, osteogenic markers, and TGFβ3 were identified, consistent with established roles in osteogenic differentiation, bone formation, calcium deposition, and transcriptional homeostasis (Guerrero et al., 2014; Zhu et al., 2024).

Single-cell transcriptomic profiling, integrated with bulk transcriptomic and proteomic analyses, demonstrated that collagen gene family members exert critical regulatory function during eggshell calcification. COL4A1 and COL4A2 encode type IV collagen α -chains that assemble into a "chicken-wire" scaffold in conjunction with laminins, proteoglycans, and entactin/nidogen. Disruption of COL4A1 impairs intracellular Ca^{2+} signaling in the smooth sarcoplasmic reticulum and contributes to age-related cerebral small vessel disease in COL4A1 mutant mice (Yamasaki et al., 2023). COL1A1 and COL1A2 encode type I collagen pro- α chains, with pathogenic

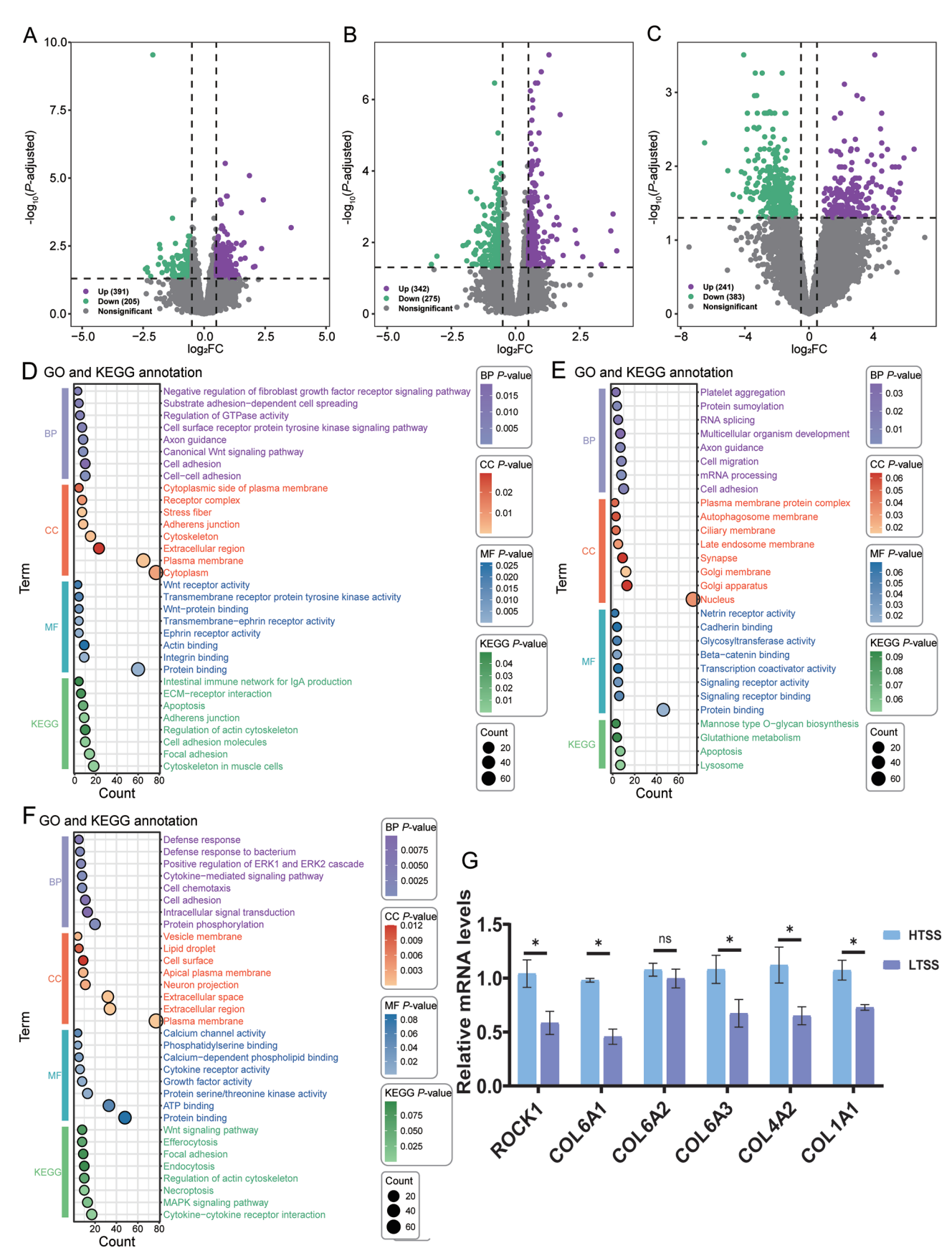


Figure 6 Transcriptomic profiling of uterus, isthmus, and duodenum

A–C: Differentially expressed gene (DEG) volcano plots for each tissue. D–F: GO and KEGG functional enrichment analyses of DEGs. G: Relative mRNA levels of different genes between high- (HTSS) and low-strength (LTSS) groups. ns: Not significant; *: P<0.05.

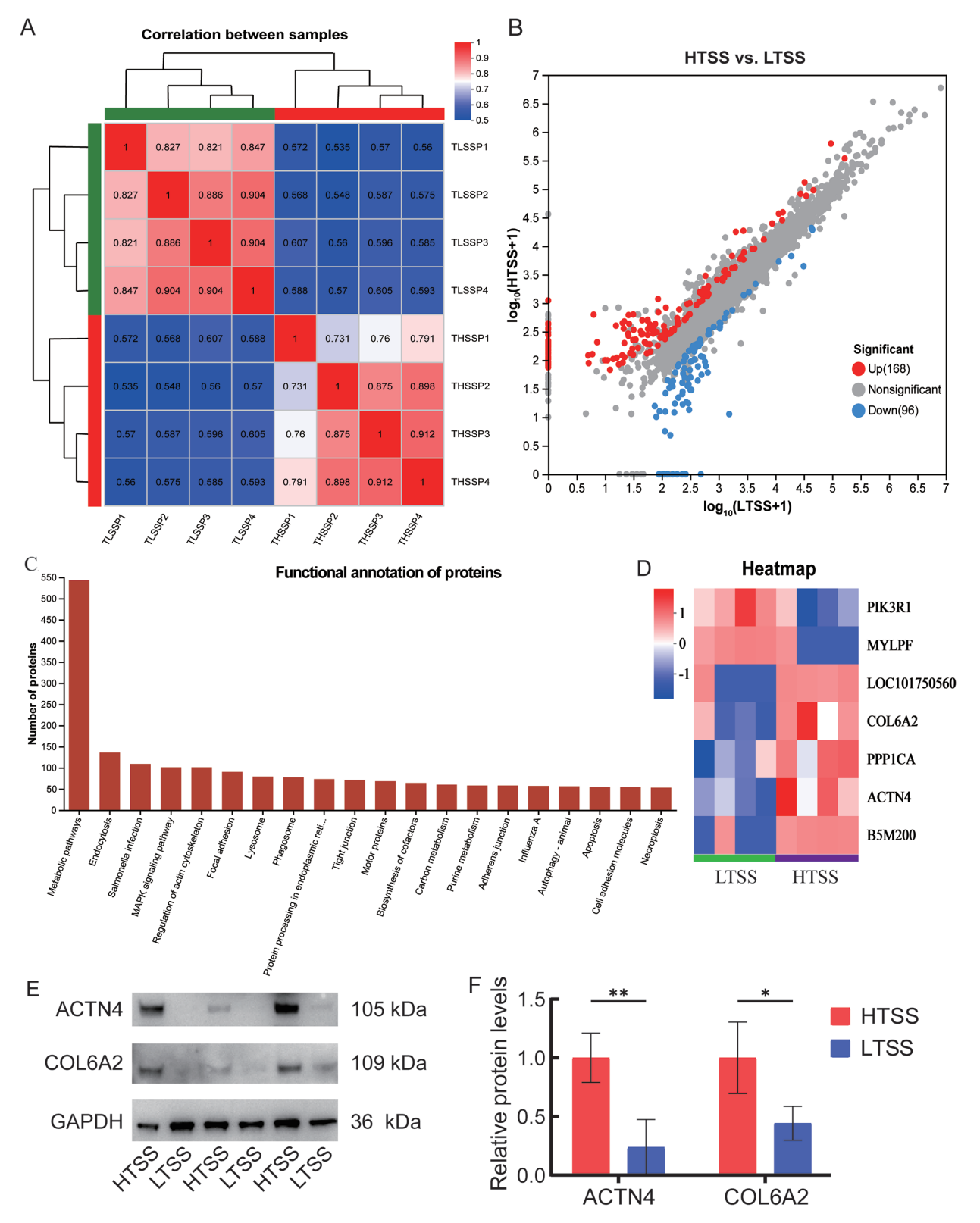


Figure 7 Proteomic analysis of uterine fluid

A: Correlation heatmap across samples. B: Volcano plot of differentially expressed proteins between high- (HTSS) and low-strength (LTSS) groups. C: KEGG pathway enrichment analysis of all proteins. D: Heatmap of differentially expressed proteins (*P*<0.05) in the focal adhesion pathway. E: Western blot analysis of uterine fluid proteins prepared from HTSS and LTSS groups. F: Relative protein levels of COL6A2 and ACTN4 in HTSS and LTSS groups. *: *P*<0.05; **: *P*<0.01.

variants implicated in human uterine diseases and osteogenesis imperfecta (Lu et al., 2023; Zhytnik et al., 2019). *COL5A1* contributes to the synthesis of low-abundance fibrillar collagen, while *COL6A1*, *COL6A2*, and *COL6A3* encode

matrix-binding collagens essential for tissue structural integrity and cellular adhesion. Functional studies have demonstrated that silencing of *COL6A1* suppresses proliferation and migration in human aortic vascular smooth muscle cells (Chen

et al., 2019). These collagen family genes (COL4A1/2, COL1A1/2, COL5A1, and COL6A1/2/3) influence eggshell strength through coordinated synthesis of matrix scaffolds and regulation of intracellular calcium ions. These findings are consistent with previous transcriptomic studies of the chicken uterus (Zhang et al., 2015) and underscore the enrichment of these genes in focal adhesion and ECM-receptor interaction pathways. Beyond calcification, collagen family members also participate in folliculogenesis, supporting structural remodeling and intercellular communication during ovarian development (Du et al., 2022; Huang et al., 2022).

Genes encoding voltage-gated calcium subunits were also implicated in eggshell strength via enrichment in calcium signaling and membrane-depolarization pathways. CACNB2 encodes the β_2 regulatory subunit of high-voltage-dependent calcium channels, while CACNA1C encodes the pore-forming α₁C subunit responsible for generating L-type calcium currents, which are involved in chondrogenesis during limb development (Atsuta et al., 2019), and has also been implicated in eggshell strength (Li et al., 2021). CACNA2D1 is involved in calcium channels that mediate calcium ion influx into the cell upon membrane depolarization. The calcium voltage-gated channel family genes (CACNB2, CACNA1C, and CACNA2D1) affect eggshell strength by controlling the voltage-gated calcium channels that generate L-type calcium currents, consistent with earlier transcriptomic studies (Zhang et al., 2015). These genes are functionally concentrated in the calcium signaling pathway and represent key modulators of uterine calcium flux during shell formation.

Annexin A5 and A6, encoded by ANXA5 and ANXA6, are calcium-dependent phospholipid-binding proteins implicated in membrane trafficking events, particularly during exocytosis and endocytosis. High levels of ANXA5 in chicken uterine fluid have been associated with increased fertilization rates (Riou et al., 2019). Integrin subunits encoded by ITGA9 and ITGB1 mediate intercellular and cell-matrix adhesion by recognizing proline-rich motifs in collagen and promoting laminin matrix deposition. These integrins can also vasoconstriction through Ca2+ influx via L-type voltage-gated channels and Rho-associated kinase-mediated calcium sensitivity (Morris et al., 2022). Solute carrier genes (SLC4A4/7, SLC6A4, SLC9A2/9, and SLC38A2) and ATPase family genes (ATP1A1, ATP1B1, ATP2B1/2, ATP2A2/3, and ATP2C1) contribute to eggshell formation by regulating the transport and homeostasis of Na+, K+, Ca2+, HCO3+, and Clions, as well as intracellular pH. These functions align with previous descriptions of uterine ion transporters involved in the initiation of eggshell calcification (Bahadoran et al., 2018; Cui et al., 2025; Gloux et al., 2019; Jonchère et al., 2012; Li et al., 2025; Zhang et al., 2022). Identification of these candidate genes provides a reference for genetic association studies on eggshell strength, and may inform the development of single nucleotide polymorphism (SNP)-based selection strategies to improve shell quality in late-phase laying hens.

Prior to the onset of calcification, the uterus lacks intrinsic calcium storage capacity. During active eggshell mineralization, calcium ions are rapidly mobilized from the bloodstream, alongside a substantial quantity of matrix proteins required for shell formation (Nys et al., 1999). In the present study, serum calcium and phosphorus concentrations were modestly elevated in the high-strength group relative to the low-strength group, consistent with previous findings that serum calcium exerts limited effects on shell strength (Zhang

et al., 2019). Dietary calcium is primarily absorbed in the duodenum, and its level significantly impacts shell quality. Increases in dietary calcium from 1.5% to 2.5% improve shell quality, although further increase beyond 2.5% yield no appreciable gains (Moreki et al., 2011; Cufadar et al., 2011). In this study, transcriptomic analysis of the duodenal tissues revealed significant enrichment of calcium channel activityrelated pathways, highlighting the regulatory linkage between absorption of Ca2+ and the release of calcium ions. Proteomic analysis of uterine fluid identified high expression of ANXA4 and ANXA5, markers associated with high fertilization ability (Riou et al., 2019), while CACNA2D3 is associated with the number of eggs laid (Lei et al., 2024). Integration of these transcriptomic and proteomic datasets suggests the ANXA2, ANXA5, and CACNA2D3 may modulate duodenal calciumchannel activity, thereby influencing Ca2+ absorption and, in turn, affecting eggshell quality.

This study expanded the repertoire of candidate genes beyond those previously reported (Zhang et al., 2022; Li et al., 2025). In addition, previously characterized functions of ion transporter genes were integrated with current findings to infer roles for newly identified genes in eggshell formation, enabling refinement of the uterine ion transport model (Figure 8).

CONCLUSION

A single-cell transcriptomic atlas of the Rhode Island Red chicken uterus was successfully constructed, resolving nine distinct cell types broadly categorized as smooth muscle. epithelial, endothelial, and immune cells. Integration of multiomics data identified six gene families-collagens, solute carriers, ATPases, calcium voltage-gated channels, annexins, and integrin subunits—as contributors to eggshell strength. These genes were predominantly associated with focal adhesion, actin cytoskeleton regulation, ECM-receptor interaction, and calcium signaling. Collagen genes were primarily expressed in smooth muscle cells, implicating these cells in matrix remodeling during eggshell calcification. This study identified key genetic factors that contribute to variation in eggshell strength in Rhode Island Red chickens, providing a mechanistic foundation for understanding the regulatory pathways that influence eggshell formation and offering a basis for strategies aimed at improving shell quality.

DATA AVAILABILITY

The single-cell sequencing data generated in this study have been deposited in the Genome Sequence Archive under PRJCA047136 (https://ngdc.cncb.ac.cn/genbase), Science Data Bank under 10.57760/sciencedb.29064 (https://www.scidb.cn/), and NCBI under BioProjectID PRJNA1335897.

SUPPLEMENTARY DATA

Supplementary data to this article can be found online.

COMPETING INTERESTS

The authors declare that they have no competing interests.

AUTHORS' CONTRIBUTIONS

X.K.Z. designed the research framework, conducted comprehensive data analysis, interpreted the results, validated data accuracy, contributed to data visualization, prepared the first draft of the manuscript, and reviewed and edited the manuscript. J.L.C. and Y.L.L. designed the research framework, secured funding, supervised the entire project, validated data accuracy, reviewed and edited the manuscript, and ensured coordination among all team members. Y.Y.S. and Q.L. suggested substantial revisions

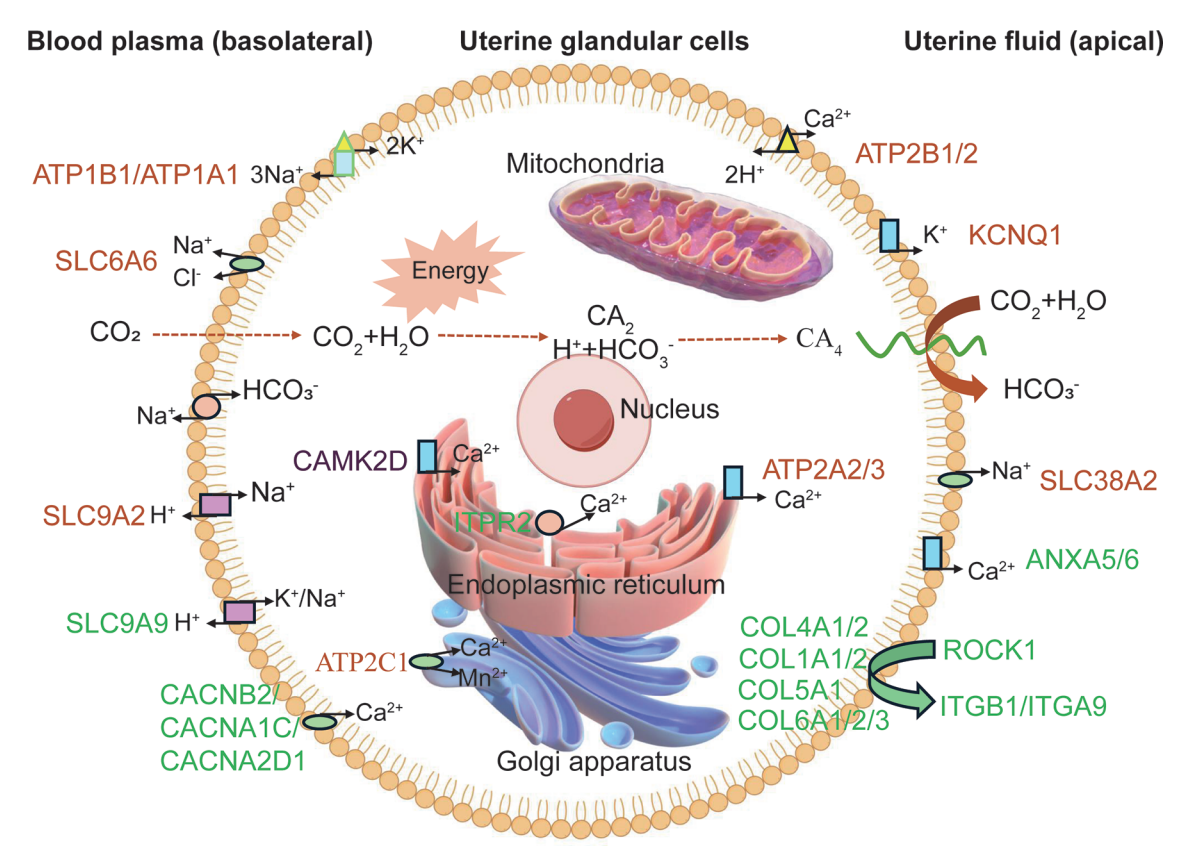


Figure 8 Proposed model of uterine ion transporters during eggshell calcification

Candidate genes up-regulated or down-regulated during calcification are highlighted in green and orange, respectively.

to improve clarity and coherence. P.Y.M., H.F.D., H.H.Y., X.Y.L., and X.Y.X. were responsible for collecting and processing samples. H.M. and J.W.Y. interpreted the results. All authors read and approved the final version of the manuscript.

REFERENCES

Ar A, Rahn H, Paganelli CV. 1979. The avian egg: mass and strength. *The Condor: Ornithological Applications*, **81**(4): 331–337.

Atsuta Y, Tomizawa RR, Levin M, et al. 2019. L-type voltage-gated Ca^{2+} channel $Ca_V 1.2$ regulates chondrogenesis during limb development. Proceedings of the National Academy of Sciences of the United States of America. **116**(43): 21592–21601.

Bahadoran S, Dehghani Samani A, Hassanpour H. 2018. Effect of heat stress on the gene expression of ion transporters/channels in the uterus of laying hens during eggshell formation. *Stress*, **21**(1): 51–58.

Bain MM, Nys Y, Dunn IC. 2016. Increasing persistency in lay and stabilising egg quality in longer laying cycles. What are the challenges?. *British Poultry Science*, **57**(3): 330–338.

Becht E, McInnes L, Healy J, et al. 2019. Dimensionality reduction for visualizing single-cell data using UMAP. *Nature Biotechnology*, **37**(1): 38–44

Bolger AM, Lohse M, Usadel B. 2014. Trimmomatic: a flexible trimmer for Illumina sequence data. *Bioinformatics*, **30**(15): 2114–2120.

Brionne A, Nys Y, Hennequet-Antier C, et al. 2014. Hen uterine gene expression profiling during eggshell formation reveals putative proteins involved in the supply of minerals or in the shell mineralization process. BMC Genomics. 15(1): 220.

Chen XM, Li XC, Zhong CH, et al. 2024. Genetic patterns and genome-wide association analysis of eggshell quality traits of egg-type chicken across an extended laying period. *Poultry Science*, **103**(4): 103458.

Chen ZX, Wu QJ, Yan CJ, et al. 2019. COL6A1 knockdown suppresses cell

proliferation and migration in human aortic vascular smooth muscle cells. Experimental and Therapeutic Medicine, 18(3): 1977–1984.

Cheng X, Ning ZH. 2023. Research progress on bird eggshell quality defects: a review. *Poultry Science*, **102**(1): 102283.

Cox J, Hein MY, Luber CA, et al. 2014. Accurate proteome-wide label-free quantification by delayed normalization and maximal peptide ratio extraction, termed MaxLFQ. *Molecular & Cellular Proteomics*, **13**(9): 2513–2526.

Cufadar Y, Olgun O, Yildiz AÖ. 2011. The effect of dietary calcium concentration and particle size on performance, eggshell quality, bone mechanical properties and tibia mineral contents in moulted laying hens. *British Poultry Science*, **52**(6): 761–768.

Cui ZF, Amevor FK, Tang BC, et al. 2025. Gga-miR-34b-3p targets calbindin 1 to regulate cellular calcium ion homeostasis during eggshell calcification in chicken uterus. *International Journal of Biological Macromolecules* **286**: 138520

Dobin A, Davis CA, Schlesinger F, et al. 2013. STAR: ultrafast universal RNA-seg aligner. *Bioinformatics*. **29**(1): 15–21.

Du HT, Guo Y, Wu XH, et al. 2022. FOXL2 regulates the expression of the *Col4a1* collagen gene in chicken granulosa cells. *Molecular Reproduction* and *Development*, 89(2): 95–103.

Gautron J, Hincke MT, Nys Y. 1997. Precursor matrix proteins in the uterine fluid change with stages of eggshell formation in hens. *Connective Tissue Research*. **36**(3): 195–210.

Gautron J, Stapane L, Le Roy N, et al. 2021. Avian eggshell biomineralization: an update on its structure, mineralogy and protein tool kit. *BMC Molecular and Cell Biology*, **22**(1): 11.

Gloux A, Le Roy N, Brionne A, et al. 2019. Candidate genes of the transcellular and paracellular calcium absorption pathways in the small intestine of laying hens. *Poultry Science*, **98**(11): 6005–6018.

Grün D, Van Oudenaarden A. 2015. Design and analysis of single-cell

sequencing experiments. Cell, 163(4): 799-810.

Guerrero F, Herencia C, Almadén Y, et al. 2014. TGF-β prevents phosphate-induced osteogenesis through inhibition of BMP and Wnt/β-catenin pathways. *PLoS One*, **9**(2): e89179.

Hincke MT, Gautron J, Panheleux M, et al. 2000. Identification and localization of lysozyme as a component of eggshell membranes and eggshell matrix. *Matrix Biology*, **19**(5): 443–453.

Huang X, Zhou W, Cao HY, et al. 2022. Ovarian transcriptomic analysis of Ninghai indigenous chickens at different egg-laying periods. *Genes*, **13**(4): 595.

Jonchère V, Brionne A, Gautron J, et al. 2012. Identification of uterine ion transporters for mineralisation precursors of the avian eggshell. *BMC Physiology*. **12**: 10.

Kim D, Paggi JM, Park C, et al. 2019. Graph-based genome alignment and genotyping with HISAT2 and HISAT-genotype. *Nature Biotechnology*, **37**(8): 907–915.

Lei QX, Zhang SE, Wang J, et al. 2024. Genome-wide association studies of egg production traits by whole genome sequencing of Laiwu Black chicken. *Poultry Science*, **103**(6): 103705.

Leng D, Zeng B, Wang T, et al. 2024. Single nucleus/cell RNA-seq of the chicken hypothalamic-pituitary-ovarian axis offers new insights into the molecular regulatory mechanisms of ovarian development. *Zoological Research*, **45**(5): 1088–1107.

Li QL, Duan ZY, Sun CJ, et al. 2021. Genetic variations for the eggshell crystal structure revealed by genome-wide association study in chickens. *BMC Genomics*, **22**(1): 786.

Li WQ, Ma XY, Li XM, et al. 2025. Integrating proteomics and metabolomics to elucidate the regulatory mechanisms of pimpled egg production in chickens. *Poultry Science*, **104**(2): 104818.

Liao Y, Smyth GK, Shi W. 2014. featureCounts: an efficient general purpose program for assigning sequence reads to genomic features. *Bioinformatics*, **30**(7): 923–930.

Liu Z, Sun CJ, Yan YY, et al. 2018. Genetic variations for egg quality of chickens at late laying period revealed by genome-wide association study. *Scientific Reports*, **8**(1): 10832.

Lu Y, Chen XY, Zeng WJ, et al. 2023. *COL1A1*: : PDGFB fusion uterine sarcoma with a *TERT* promoter mutation. *Genes, Chromosomes and Cancer*, **63**(1): e23210.

Marečková M, Garcia-Alonso L, Moullet M, et al. 2024. An integrated single-cell reference atlas of the human endometrium. *Nature Genetics*, **56**(9): 1925–1937.

Martinez-Val A, Bekker-Jensen DB, Hogrebe A, et al. 2021. Data processing and analysis for dia-based phosphoproteomics using spectronaut. *Methods in Molecular Biology*, **2361**: 95–107.

McGinnis CS, Murrow LM, Gartner ZJ. 2019. DoubletFinder: doublet detection in single-cell RNA sequencing data using artificial nearest neighbors. *Cell Systems*, **8**(4): 329–337. e4.

Moreki JC, Van Der Merwe HJ, Hayes JP. 2011. Effect of dietary calcium level on egg production and eggshell quality in broiler breeder hens from 36 to 60 weeks of age. *Online Journal of Animal and Feed Research*, **1**(1): 1–7.

Morris GE, Denniff MJ, Karamanavi E, et al. 2022. The integrin ligand SVEP1 regulates GPCR - mediated vasoconstriction via integrins $\alpha 9\beta 1$ and $\alpha 4\beta 1$. *British Journal of Pharmacology*, **179**(21): 4958–4973.

Nys Y, Hincke MT, Arias JL, et al. 1999. Avian eggshell mineralization. *Poultry and Avian Biology Reviews*, **10**(3): 143–166.

Riou C, Brionne A, Cordeiro L, et al. 2019. Proteomic analysis of uterine fluid of fertile and subfertile hens before and after insemination. *Reproduction*, **158**(4): 335–356.

Roland M Jr L. 1982. Biochemistry of the organic matrix of the eggshell. *Poultry Science*, **61**(10): 2040–2047. Shapiro MD, Kronenberg Z, Li C, et al. 2013. Genomic diversity and evolution of the head crest in the rock pigeon. *Science*, **339**(6123): 1063–1067.

Silversides FG, Shaver DM, Song Y. 2007. Pure line laying chickens at the Agassiz Research Centre. *Animal Genetic Resources Information*, **40**: 79–85.

Soledad Fernandez M, Moya A, Lopez L, et al. 2001. Secretion pattern, ultrastructural localization and function of extracellular matrix molecules involved in eggshell formation. *Matrix Biology*, **19**(8): 793–803.

Sun CJ, Qu L, Yi GQ, et al. 2015. Genome-wide association study revealed a promising region and candidate genes for eggshell quality in an F_2 resource population. *BMC Genomics*, **16**(1): 565.

Sun CJ, Xu GY, Yang N. 2013. Differential label - free quantitative proteomic analysis of avian eggshell matrix and uterine fluid proteins associated with eggshell mechanical property. *Proteomics*, **13**(23-24): 3523–3536.

Sun TT, Xiao C, Yang ZL, et al. 2023. Transcriptome profiling analysis of uterus during chicken laying periods. *BMC Genomics*, **24**(1): 433.

Takahashi H, Sasaki O, Nirasawa K, et al. 2010. Association between ovocalyxin - 32 gene haplotypes and eggshell quality traits in an F_2 intercross between two chicken lines divergently selected for eggshell strength. *Animal Genetics*, **41**(5): 541–544.

Takahashi H, Yang D, Sasaki O, et al. 2009. Mapping of quantitative trait loci affecting eggshell quality on chromosome 9 in an F_2 intercross between two chicken lines divergently selected for eggshell strength. *Animal Genetics*, **40**(5): 779–782.

Wang T, Leng D, Cai ZK, et al. 2024. Insights into left-right asymmetric development of chicken ovary at the single-cell level. *Journal of Genetics and Genomics*, **51**(11): 1265–1277.

Wang WX, Vilella F, Alama P, et al. 2020. Single-cell transcriptomic atlas of the human endometrium during the menstrual cycle. *Nature Medicine*, **26**(10): 1644–1653.

Yamasaki E, Thakore P, Ali S, et al. 2023. Impaired intracellular Ca²⁺ signaling contributes to age-related cerebral small vessel disease in *Col4a1* mutant mice. *Science Signaling*, **16**(811): eadi3966.

Yang R, Geng F, Huang X, et al. 2020. Integrated proteomic, phosphoproteomic and N-glycoproteomic analyses of chicken eggshell matrix. *Food Chemistry*, **330**: 127167.

Zhang JC, Wang YN, Zhang C, et al. 2019. The differences of gonadal hormones and uterine transcriptome during shell calcification of hens laying hard or weak-shelled eggs. *BMC Genomics*, **20**(1): 707.

Zhang Q, Zhu F, Liu L, et al. 2015. Integrating transcriptome and genome re-sequencing data to identify key genes and mutations affecting chicken eggshell qualities. *PLoS One*, **10**(5): e0125890.

Zhang XK, Li YL, Li Q, et al. 2024. Research Note: genetic parameters estimation of egg quality traits in rhode island red and white leghorn chickens. *Poultry Science*, **103**(12): 104263.

Zhang ZC, Du XX, Lai S, et al. 2022. A transcriptome analysis for 24-hour continuous sampled uterus reveals circadian regulation of the key pathways involved in eggshell formation of chicken. *Poultry Science*, **101**(1): 101531.

Zhao DR, Gao LB, Gong F, et al. 2024. TMT-based quantitative proteomic analysis reveals eggshell matrix protein changes correlated with eggshell quality in Jing Tint 6 laying hens of different ages. *Poultry Science*, **103**(3): 103463.

Zhu SY, Chen W, Masson A, et al. 2024. Cell signaling and transcriptional regulation of osteoblast lineage commitment, differentiation, bone formation, and homeostasis. *Cell Discovery*, **10**(1): 71.

Zhytnik L, Maasalu K, Pashenko A, et al. 2019. *COL1A1/2* pathogenic variants and phenotype characteristics in Ukrainian osteogenesis imperfecta patients. *Frontiers in Genetics*, **10**: 722.